DYNAMIC SIMULATIONS OF ELASTIC RODS FOR MEDICAL APPLICATIONS

A Thesis

by

SRAVANI NUTI

Submitted to the Office of Graduate and Professional Studies of
Texas A&M University
in partial fulfillment of the requirements for the degree of

MASTER OF SCIENCE

Chair of Committee,	J. N. Reddy
Co-Chair of Committee,	Annie Ruimi
Committee Member,	Arun Srinivasa
Head of Department,	A. A. Polycarpou

December 2014

Major Subject: Mechanical Engineering

ABSTRACT

This study deals with a detailed development of a computational model based on the Cosserat rod theory to describe the motion of elastic filaments such as threads and hair. The need for a simulation software for the act of suturing has motivated this study.

The dynamic equations governing the motion of elastic rods have been solved using a finite difference scheme. The scheme is central difference in space and forward difference in time and is conditionally stable. The simulations are carried out for a cantilever beam for various force and moment inputs at its free end. The results have been validated using known analytical results. The scheme has proven to be fast enough to be used in real-time simulations.

To my parents

ACKNOWLEDGEMENTS

I would like to thank my committee chair, Dr. J. N. Reddy, and co-chair, Dr. Annie Ruimi for their guidance and support throughout the course of this research. I would also like to thank my committee member, Dr. Arun Srinivasa for his motivation and advice.

This work was made possible by the NPRP award 5-353-2-138 from the Qatar National Research Fund, a member of the Qatar Foundation. The statements made herein are solely the responsibility of the authors.

Thanks also go to my friends and colleagues and the department faculty and staff for making my time at Texas A&M University a great experience.

Finally, I would like to thank my family for their encouragement and support.

NOMENCLATURE

$\{\mathbf{e}_1, \mathbf{e}_2, \mathbf{e}_3\}$	Fixed reference frame
$\{\mathbf{d}_1, \mathbf{d}_2, \mathbf{d}_3\}$	Moving reference frame
s	Arc length (m)
t	Time (s)
L	Length of rod (m)
T	Total time considered (s)
d	Diameter of rod (m)
ρ	Density of rod (kg/m^3)
$m(s)$	Mass per unit length (kg/m)
$\tilde{\mathbf{I}}(s)$	Principal mass moment of inertia tensor (kg/m^2)
E	Modulus of elasticity (N/m^2)
G	Torsional rigidity modulus (N/m^2)
$\mathbf{B}$	Stiffness tensor (N-m^2)
$\mathbf{R}(s,t)$	Centerline position vector (m)
$\mathbf{v}(s,t)$	Linear velocity (m/s)
$\boldsymbol{\omega}(s,t)$	Angular velocity (rad/s)
$\mathbf{M}(s,t)$	Contact moment (N-m)
$\mathbf{u}(s,t)$	Darboux vector (m^{-1})

$\mathbf{u_0}(s,t)$	Initial Darboux vector (m^{-1})
$\mathbf{N}(s,t)$	Contact force (N)
$\mathbf{T}(s,t)$	External force (N)
$\mathbf{Q}(s,t)$	External moment (N-m)
I_1	Second moment of inertia about $\mathbf{d_1}$
I_2	Second moment of inertia about $\mathbf{d_2}$
J	Second moment of inertia about $\mathbf{d_3}$

TABLE OF CONTENTS

Page

ABSTRACT ii

DEDICATION iii

ACKNOWLEDGEMENTS iv

NOMENCLATURE v

TABLE OF CONTENTS vii

LIST OF FIGURES viii

LIST OF TABLES ix

1. INTRODUCTION 1

2. LITERATURE REVIEW 4

3. THEORETICAL FORMULATION OF RODS 8

3.1 Definitions 8
3.2 Governing Equations 10
3.3 Compatibility Equation 12
3.4 Constraint Equation 13
3.5 Summary of Equations 14

4. MATHEMATIC FORMULATION 15

4.1 Introduction 15
4.2 Numerical Algorithm 16

5. RESULTS 21

5.1 Preliminaries 21
5.2 Simulation Results 22

6. CONCLUSION 33

REFERENCES 34

LIST OF FIGURES

Page

Figure 1: Free body diagram of an infinitesimal element of the rod. 10

Figure 2: Suture thread fixed at the skin and subjected to forces and moments via the needle. [20]. 16

Figure 3: Snapshots of the filament's final configuration (right) (at the last time step) for different inputs (left): (a) Only N_1 [22], (b) M_1 and M_2 [23]. 23

Figure 4: Buckling of the rod under: (a) Axial force [24], (b) Twisting moment [25]. 24

Figure 5: Effect of elasticity modulus on buckling due to twist. 26

Figure 6: Effect of length on buckling due to twist. 27

Figure 7: Effect of rod diameter on twisting moment causing buckling. 27

Figure 8: Effect of rod length on axial force required to buckle the rod. 28

Figure 9: Effect of diameter on the axial force required to buckle the rod. 29

Figure 10: Transient response of the rod due to an impulse force [28]. 30

Figure 11: Predicted values of displacement as a function of time (left) and simulated values (right). 31

Figure 12: FFT analysis of motion at free end of the rod. 31

Figure 13: FFT analysis of motion at mid-point of the rod. 32

LIST OF TABLES

Page

Table 1: Table with properties and their values. 21

Table 2: Analytical vs simulated results. 24

1. INTRODUCTION

In the 21st century, the digital age, everything we do has been made easier or more efficient using computers. The affordability of personal computers and the development of computer graphics have improved user experience with interactive games and 3-D movies. It has also helped in developing software for the engineering field to design mechanical components, predict failure and the like.

In games and animated movies, the need to represent the motion of hair and clothes more realistically has spurred the interest in the mechanics of thin elastic rods. In these fields, however, the visualization aspect of the motion of these systems is more important than the accuracy of it. Fields, such as oil and gas and bio-medical engineering use the design of flexible structures such as wires, cables, ropes, threads, grape vines, and DNA polymers. Here, the accuracy of reaction forces and displacements of the rod play a major role.

In the last few years, there have been efforts to use computer simulations in medical fields to help train students in the art of suturing. The present methods of training use cadavers, animal carcasses, foam models and the like [1]. These do not accurately represent the real situation and hence newer methods are being looked into. Initially, most of the effort was spent in modeling tissues and organs [2] than the surgical instruments used in suturing, such as the suture threads and needle. Keeping up with the need for a surgical simulation software, therefore, it is now important to simulate the

behavior of the surgical thread during the process of suturing in a surgery. Suture threads, undergoing complex movements as stitching, knotting, and cutting, are examples of thin deformable bodies exhibiting twisting, bending, and buckling due to different forces and moments. The present study aims to model accurately the motion of the suture thread in real-time so as to be used in a surgical training software.

The simplest choice for modeling these thin rods is to use the Euler-Bernoulli theory [3,4], which, unlike the Timoshenko beam theory [3,4], does not take into account the shear deformation and rotational inertia effects. In 1859, Kirchhoff [5] first presented a rod theory that assigned each point of the rod six degrees of freedom - three translational and three rotational, so that both bending and torsion could be modeled. But the theory assumes that the rod is inextensible, the material behavior is linear, and the shear deformation is negligible. The Cosserat continuum theory [6] is one of the most prominent extended continuum theories. With the assumption of small strains, it resembles the Kirchhoff-Clebsh theory. The classical infinitesimal volume element of continuum mechanics is subjected to only volume and surface forces, whereas the Cosserat volume element involves a gradient of forces and a surface couple on each edge. Like the Kirchhoff theory, it treats each point on the rod as rigid having 6 degrees of freedom, three displacements and three rotations. Each point is assigned a triad of directors ($\mathbf{d}_i$, i=1, 2, 3) and the rate of change of these directors in time and space describe the motion of the rod.

The present study is restricted to inextensible rods that do not undergo shear deformation. This results in two constraint equations which along with the equations of motion form a system of non-linear partial differential equations. Thus, the overall objective of this study is to formulate a method that can solve this set of equations accurately and quickly so as to be used in real-time simulations.

In the section following this introduction, the methods implemented previously to solve similar problems will be presented. In section 3, the theoretical formulation of the rod will be described in more detail and the governing equations derived. In section 4, the method used to solve the derived equations is presented. In section 5, the results from the computer implementation of the method are shown with a brief discussion on them. The study is concluded with a brief summary of work and its future possibilities.

2. LITERATURE REVIEW

In 2002, Pai [7] modeled thin elastic bodies that are inextensible and do not undergo shear, fixed at one end and subjected to force and moment inputs at the other end. This model can be used to represent the statics of catheters, sutures, tendons, hair, etc. The coupled boundary value differential equations were solved in two sweeps, from the free end to the fixed end, calculating the stresses and strains and then from the fixed end to the free end calculating the position and rotation at each point of the rod. This method offered an effective approach that could animate continuous thin deformable bodies in a physically correct way. However, the system handled only statics and self-contact had not been considered.

A finite difference scheme, unconditionally stable, called generalized alpha method was used by Goyal, Perkins, and Lee [8] to solve the coupled partial differential equations obtained from the continuum rod model. The scheme was used to simulate the dynamics of DNA filaments. Avoiding the singularities arising from the use of Euler angles to track large rotations, incremental rotations were used. The boundary conditions were solved for using shooting method, but its implementation is not very efficient in non-linear problems. Self-contact and intertwining were also modeled.

Sobottka, Lay, and Weber [9] used the generalized alpha method to model hair. The boundary conditions were solved using a relaxation technique and employing the classical Newton iteration instead of the shooting method used by Goyal, Perkins, and

Lee [8]. The method is stable even with larger time steps and is relatively easy to follow. Gobat and Grosenbaugh [10] also used a similar method to solve a problem of oceanographic mooring. The Newton-Raphson method [11] was used to solve the system of equations. Solving equations using the Newton method may pose a convergence problem for certain cases. And with the use of generalized alpha method, the selection of parameters that will make the scheme unconditionally stable seems to be more or less trial and error and may have to be changed for different problems.

A numerically stable finite difference method was presented by Lang, Linn, and Arnold [12] to model the dynamic response of Cosserat rods. A staggered grid was used for the approximation and quaternions used to represent rotations. The evolution of these quaternions was used to compute the curvatures of the rod. The scheme, being fast, can be used in real-time simulations. Collisions and interactions with other media are yet to be modeled.

In addition to finite difference methods to solve the dynamic equations, finite element methods (FEM) have also been widely used. FEM has been used to model organs previously, however it is found to be relatively time consuming when it comes to modeling sutures. This is because a fine mesh is required to capture the rod configuration in space and at each node there are a large number of parameters. Spillmann and Teschner [13] introduced a visually suitable method, where a finite element method was used to calculate the restoration forces and torques in every element

and then, using these values, the displacements and rotations of the centerline were computed. Rotations were represented as quaternions.

Cao, Liu, and Wang [14] used finite element method as well to model the dynamics of 3-dimensional slender structures using a Cosserat rod element formulation. Approximate solutions to the non-linear partial differential equations of motion in quasi-static sense were used as shape functions. These functions were up to third order in nodal displacements and gave a more accurate dynamic response even with a coarser mesh.

Another interesting approach was developed by Berkley et al. [15] where the problem of higher computation time was solved using a constraints approach. Here, the unknowns are calculated on a need to know basis. That is, interior nodes are ignored as the displacements there are not needed and the reaction forces calculated only where contact occurs. This condenses the stiffness matrix and hence reduces time required for computation. However, non-linear material properties and large deformation formulations were yet to be considered.

Other approaches to model thin elastic structures include using spring-mass systems and spline-based models. Brown, Latombe, and Montgomery [16] and Wang et al. [17] used spring-mass systems; the former could only model bending whereas Wang linked each element with torsional springs to handle twist too. However, these methods are not based on the continuum approach. Hadap and Thalmann [18] represented a rod as a chain of rigid bodies and included twist dynamics into the differential algebraic

equations. But the computation is time consuming and hence may not be well suited for virtual reality simulations. An example for spline-based model is the work of Lenoir et al [19], where sliding point constraints on a spline along with continuum mechanics were used to simulate the movement of the thread through skin.

In the present study, we want to develop a physics-based numerical method to solve the dynamic equations of Cosserat rod theory which can be used to simulate the behavior of suture threads.

3. THEORETICAL FORMULATION OF RODS*

This section describes the physics of the motion of the thin elastic rods. The Cosserat rod theory is chosen to model the rods with the assumptions that the rod is inextensible and it does not undergo shear. The nomenclature used and the derivation of the governing equations are presented below.

3.1 Definitions

A rod is a structure whose one dimension is relatively much bigger than the other dimensions. It can experience extension, twisting and bending. One can treat each point of the rod as a rigid body and with the conservation of linear and angular momentum of each of these points; the dynamic behavior of the rod may be developed.

Let us consider a rod of length, *L*, in space, whose coordinates are represented by the orthonormal system, $\{\mathbf{e_1}, \mathbf{e_2}, \mathbf{e_3}\}$. Suppose the rod is subjected to various forces, $\mathbf{T}(s,t)$ and moments $\mathbf{Q}(s,t)$ per unit length varying with time, *t* and arc length, *s*. We shall consider the locus of the centers of mass of each cross-section as the centerline of the rod. Suppose the rod deforms such that its centerline may be represented as a three-dimensional curve, $\mathbf{R}(s,t)$. Suppose a set of directors, $\{\mathbf{d_1}, \mathbf{d_2}, \mathbf{d_3}\}$ is assigned to each point on the curve, such that $\mathbf{d_1}$ and $\mathbf{d_2}$ are in the plane of the cross-section of the rod

* Parts of this chapter have been reprinted with the permission from "Modeling the dynamics of filaments for medical applications", by Nuti S., Ruimi A., Reddy J., 2014, *International Journal of Non-Linear Mechanics*, 66 (2014), 139-148, Copyright [2014] by Elsevier.

and $\mathbf{d_3}$ is normal to the cross-section. This set of directors form an orthonormal set of vectors if the rod is inextensible and does not shear. The evolution of this director frame in time and space yields the angular velocity, $\boldsymbol{\omega}$ and the curvature and twist vector, $\mathbf{u}$ (with u_1 and u_2 being the curvature components and u_3 being the twist component) respectively. The vector $\mathbf{u}$ is also called the Darboux vector. Thus the directors can be described as functions of themselves as follows:

$$\begin{cases} \left(\frac{\partial \mathbf{d_i}}{\partial s}\right)_{\mathbf{e_i}} = \mathbf{u} \times \mathbf{d_i} \\ \left(\frac{\partial \mathbf{d_i}}{\partial t}\right)_{\mathbf{e_i}} = \boldsymbol{\omega} \times \mathbf{d_i} \end{cases} \quad \textit{(i = 1,2,3).} \tag{3.1}$$

The relation between the partial derivatives of any vector, $\mathbf{a}$, with respect to a moving reference frame and the fixed frame is given by the equations:

$$\begin{aligned} \left(\frac{\partial \mathbf{a}}{\partial t}\right)_{\mathbf{d_i}} &= \left(\frac{\partial \mathbf{a}}{\partial t}\right)_{\mathbf{e_i}} - \boldsymbol{\omega} \times \mathbf{a} \\ \left(\frac{\partial \mathbf{a}}{\partial s}\right)_{\mathbf{d_i}} &= \left(\frac{\partial \mathbf{a}}{\partial s}\right)_{\mathbf{e_i}} - \mathbf{u} \times \mathbf{a} \end{aligned} \tag{3.2}$$

The free body diagram of an infinitesimal element of the rod stated above is as shown in figure 1; $\tilde{\mathbf{I}}(s)$, given as $\tilde{\mathbf{I}}(s) = \tilde{I}_1 \mathbf{d}_1 \otimes \mathbf{d}_1 + \tilde{I}_2 \mathbf{d}_2 \otimes \mathbf{d}_2 + \tilde{I}_3 \mathbf{d_3} \otimes \mathbf{d_3}$ and $m(s)$ are the tensor of principal mass moments of inertia and the mass per unit arc length of the rod respectively.

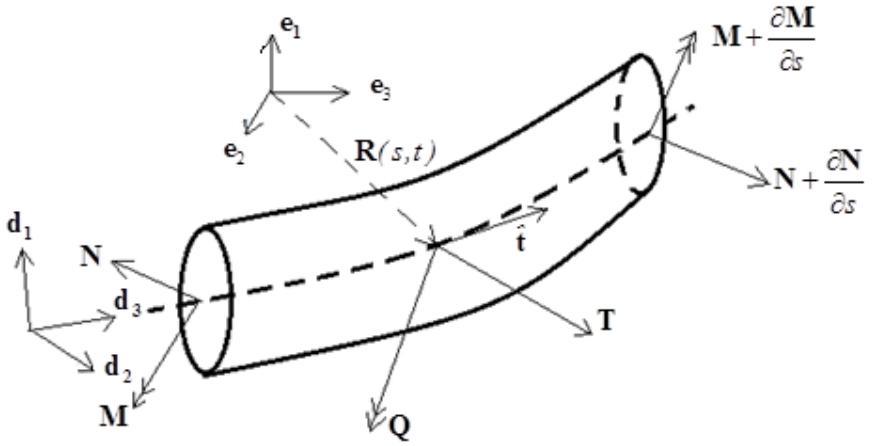

Figure 1: Free body diagram of an infinitesimal element of the rod.

All the vectors in the figure 1 are in terms of the director frame, $\{\mathbf{d_1}, \mathbf{d_2}, \mathbf{d_3}\}$. In other words, the contact force, $\mathbf{N}(s,t)$ is given as, $\mathbf{N}(s,t) = N_1\mathbf{d_1} + N_2\mathbf{d_2} + N_3\mathbf{d_3}$, with components, N_1 and N_2 being the shear forces and N_3 the axial force. Similarly, we have the contact moment, $\mathbf{M}(s,t) = M_1\mathbf{d_1} + M_2\mathbf{d_2} + M_3\mathbf{d_3}$, with M_1 and M_2 representing bending moments and M_3 representing the twisting moment, $\mathbf{L}$ is the resultant external torque per unit arc length, which includes the applied torque, $\mathbf{Q}$ and the torque due to the applied force, $\mathbf{T}$. $\hat{\mathbf{t}}$ is the tangent at the point being considered.

3.2 Governing Equations

The conservation of linear and angular momentum for the above element gives us equations $(3.3)_1$ and $(3.3)_2$, respectively.

$$\left(\frac{\partial \mathbf{N}}{\partial s}\right)_{\{\mathbf{e_i}\}} + \mathbf{T} = m\left(\frac{\partial \mathbf{v}}{\partial t}\right)_{\{\mathbf{e_i}\}}$$
$$\left(\frac{\partial \mathbf{M}}{\partial s}\right)_{\{\mathbf{e_i}\}} + \hat{\mathbf{t}} \times \mathbf{N} + \mathbf{L} = \left(\frac{\partial \tilde{\mathbf{I}}.\boldsymbol{\omega}}{\partial t}\right)_{\{\mathbf{e_i}\}} . \tag{3.3}$$

where $\mathbf{v}(s,t)$ is the velocity vector . The restoring moment, $\mathbf{M}$ is governed by material properties of the rod and can be written using the linear constitutive equation as

$$\mathbf{M} = \mathbf{B}\left(\mathbf{u} - \mathbf{u_0}\right). \tag{3.4}$$

where, $\mathbf{u_0}$ is the vector representing the initial configuration of the rod. Presently, we shall assume that the rod is straight initially and hence, $\mathbf{u_0} = 0$. **B** is the matrix with the material properties as given below:

$$\mathbf{B} = \begin{pmatrix} B_1 & 0 & 0 \\ 0 & B_2 & 0 \\ 0 & 0 & C \end{pmatrix}. \tag{3.5}$$

Here B_1 $(= EI_1)$ and B_2 $(= EI_2)$ are the bending stiffness and C $(= GJ)$ is the torsional stiffness of the rod. E is the modulus of elasticity, G the shear modulus, I_1 and I_2 are the second moment of inertia about $\mathbf{d_1}$ and $\mathbf{d_2}$ respectively and J is the polar moment of inertia. We shall consider a rod of circular cross-section of diameter, *d*, with $I_1 = I_2 = I = \frac{\pi d^4}{64}$ and $J = \frac{\pi d^4}{32}$.

With the assumption that the rod does not shear, we can rewrite the tangent as the $\mathbf{d}_3$ vector. Thus, using equations (3.2) and (3.4), we can rewrite equation (3.3) with derivatives with respect to the moving reference frame as

$$\begin{aligned}
&\left(\frac{\partial \mathbf{N}}{\partial s}\right)_{\{\mathbf{d}_i\}} + \mathbf{u}\times\mathbf{N} + \mathbf{T} = m\left(\frac{\partial \mathbf{v}}{\partial t}\right)_{\{\mathbf{d}_i\}} + m(\boldsymbol{\omega}\times\mathbf{v}) \\
&\left(\frac{\partial(\mathbf{Bu})}{\partial s}\right)_{\{\mathbf{d}_i\}} + \mathbf{u}\times(\mathbf{Bu}) + \mathbf{d}_3\times\mathbf{N} + \mathbf{L} = \tilde{\mathbf{I}}.\left(\frac{\partial \boldsymbol{\omega}}{\partial t}\right)_{\{\mathbf{d}_i\}} + \boldsymbol{\omega}\times(\tilde{\mathbf{I}}.\boldsymbol{\omega}).
\end{aligned} \tag{3.6}$$

From now on, the subscript $\{\mathbf{d}_i\}$ shall be omitted for derivatives in the moving reference frame.

3.3 Compatibility Equation

With the use of a moving reference frame to denote the vectors, one must impose that the vectors in one frame be compatible with those in the other reference frames. Suppose **L** is the transformation matrix from $\{\mathbf{e}_i\}$ to $\{\mathbf{d}_i\}$. This can be written as

$$\begin{aligned}
&\{\mathbf{e}_i\} = \mathbf{L}^T\{\mathbf{d}_i\} \\
&\Rightarrow \mathbf{e}_i = L_{1i}\,\mathbf{d}_1 + L_{2i}\,\mathbf{d}_2 + L_{3i}\,\mathbf{d}_3 = \mathbf{L}_i.
\end{aligned} \tag{3.7}$$

Differentiating the above equation in space and time, and noting that $\{\mathbf{e}_i\}$ is a fixed frame and hence its derivatives are zero, we have

$$\frac{\partial \mathbf{L}_i}{\partial t} = -\boldsymbol{\omega}\times\mathbf{L}_i \qquad \frac{\partial \mathbf{L}_i}{\partial s} = -\mathbf{u}\times\mathbf{L}_i. \tag{3.8}$$

The compatibility condition given by equation (3.10), follows from the continuity (in space and time) of the transformation matrix, **L**. Continuity implies that the order of differentiation of $\mathbf{L_i}$ must not matter.

$$\begin{aligned} &\frac{\partial}{\partial s}\left(\frac{\partial \mathbf{L_i}}{\partial t}\right)=\frac{\partial}{\partial t}\left(\frac{\partial \mathbf{L_i}}{\partial s}\right). \\ &\Rightarrow\left[\frac{\partial \mathbf{u}}{\partial t}-\frac{\partial \boldsymbol{\omega}}{\partial s}-\mathbf{u}\times\boldsymbol{\omega}\right]\times\mathbf{L_i}=0. \end{aligned} \tag{3.9}$$

$$\Rightarrow \frac{\partial \mathbf{u}}{\partial t}-\frac{\partial \boldsymbol{\omega}}{\partial s}-\mathbf{u}\times\boldsymbol{\omega}=0. \tag{3.10}$$

3.4 Constraint Equation

The inextensibility of the rod requires the length of any infinitesimally small element be the same after and before deformation.

$$\frac{ds}{dX}=1. \tag{3.11}$$

As previously stated, if the rod is assumed to have not undergone any shear, the tangent to the centerline at any point on the curve will coincide with the vector $\mathbf{d_3}$ at that point.

$$\frac{\partial \mathbf{R}}{\partial X}=\mathbf{d_3}. \tag{3.12}$$

As stated in section 3.3 above for **L**, the continuity of **R** in space, *X* and time, *t*, implies that the order of differentiation should not matter. Using equations (3.11) and (3.12), we have

$$\frac{\partial}{\partial s}\left(\frac{\partial \mathbf{R}}{\partial t}\right)_{\{\mathbf{e_i}\}} = \frac{\partial}{\partial t}\left(\frac{\partial \mathbf{R}}{\partial s}\right)_{\{\mathbf{e_i}\}}.$$
$$\Rightarrow \left(\frac{\partial \mathbf{v}}{\partial s}\right)_{\{\mathbf{e_i}\}} = \left(\frac{\partial \mathbf{d_3}}{\partial t}\right)_{\{\mathbf{e_i}\}}. \qquad (3.13)$$

$$\Rightarrow \frac{\partial \mathbf{v}}{\partial s} + \mathbf{u}\times\mathbf{v} = \boldsymbol{\omega}\times\mathbf{d_3}. \qquad (3.14)$$

3.5 Summary of Equations

The equations (3.14), (3.10), $(3.6)_2$ and $(3.6)_1$ form the system of equations that must be solved to obtain the dynamic behavior of the rod. In a condensed form they can be written as

$$\bar{\mathbf{M}}\frac{\partial \mathbf{Y}}{\partial t} + \mathbf{K}\frac{\partial \mathbf{Y}}{\partial s} + \mathbf{F} = 0. \qquad (3.15)$$

where, $\mathbf{Y} = \{\mathbf{v}, \boldsymbol{\omega}, \mathbf{u}, \mathbf{N}\}^T$ and

$$\bar{\mathbf{M}} = \begin{bmatrix} \mathbf{0} & \mathbf{0} & \mathbf{0} & \mathbf{0} \\ \mathbf{0} & \mathbf{0} & \mathbf{I} & \mathbf{0} \\ \mathbf{0} & \tilde{\mathbf{I}} & \mathbf{0} & \mathbf{0} \\ m\mathbf{I} & \mathbf{0} & \mathbf{0} & \mathbf{0} \end{bmatrix} \quad \mathbf{K} = -\begin{bmatrix} \mathbf{I} & \mathbf{0} & \mathbf{0} & \mathbf{0} \\ \mathbf{0} & \mathbf{I} & \mathbf{0} & \mathbf{0} \\ \mathbf{0} & \mathbf{0} & \mathbf{B} & \mathbf{0} \\ \mathbf{0} & \mathbf{0} & \mathbf{0} & \mathbf{I} \end{bmatrix} \quad \mathbf{F} = \begin{Bmatrix} \boldsymbol{\omega}\times\mathbf{d_3} - \mathbf{u}\times\mathbf{v} \\ -\mathbf{u}\times\boldsymbol{\omega} \\ \boldsymbol{\omega}\times(\tilde{\mathbf{I}}.\boldsymbol{\omega}) - \mathbf{u}\times(\mathbf{B}\mathbf{u}) - \mathbf{d_3}\times\mathbf{N} - \mathbf{L} \\ m(\boldsymbol{\omega}\times\mathbf{v}) - \mathbf{u}\times\mathbf{N} - \mathbf{T} \end{Bmatrix}.$$

….. (3.16)

where **I** denotes the 3×3 identity matrix.

4. MATHEMATIC FORMULATION*

This section describes the specific problem that is solved and the method used to solve it. The finite difference scheme chosen is central in space and forward in time. Along with the equations described in the previous section, the motion of the rod is obtained using the Rodrigues formula [9, 21]. The details of the scheme and the algorithm used are presented in this section.

4.1 Introduction

The system of equations listed in the previous section, equation (3.15), is solved for a cantilever beam that is fixed at one end and is subjected to forces and moments at the free end. This mimics the scenario where the suture thread is embedded into the skin at one end and the other end is controlled by the movement of the needle as shown in the figure 2.

The selected problem is solved using a finite difference scheme that is central in space and forward in time. The scheme is conditionally stable, with the time and space step related by the transverse wave speed of the rod. Details of the scheme will be described in the following sub-section.

* Parts of this chapter have been reprinted with the permission from "Modeling the dynamics of filaments for medical applications", by Nuti S., Ruimi A., Reddy J., 2014, *International Journal of Non-Linear Mechanics*, 66 (2014), 139-148, Copyright [2014] by Elsevier.

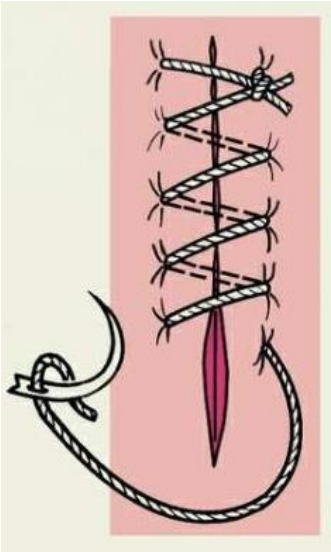

Figure 2: Suture thread fixed at the skin and subjected to forces and moments via the needle. [20].

4.2 Numerical Algorithm

Suppose the number of space points on the rod is given as *NS* and the number of points in time as *NT*. The index '*i*' is used to describe a point in space, where $i = 1$ denotes the end that is fixed ($s = 0$) and $i = NS$ denotes the free end ($s = L$). Similarly, the index '*j*' is used to denote the points in time with $j = 1$ being the starting point in time ($t = 0$) and $j = NT$ is the final point in time ($t = T$). The system of equations is solved to calculate the 4 unknowns, $\mathbf{v}, \boldsymbol{\omega}, \mathbf{u}$ and $\mathbf{N}$ at all space and time points. Each vector having 3 components, the unknowns are of the dimension $3 \times NS \times NT$. The number of space steps and time steps are not independent of each other but are related by the transverse wave speed, c_T in the rod. Let the length of each space step and time step be

denoted as Δs and Δt respectively. These can be calculated as shown in equation (4.1). The relation between them is given by equation (4.2).

$$\Delta t = \frac{T}{NT-1} \quad \text{and} \quad \Delta s = \frac{L}{NS-1} \tag{4.1}$$

$$\Delta t < \frac{\Delta s}{c_T}, \quad \text{where} \quad c_T = \frac{C(n)}{L}\sqrt{\frac{EJ}{m}} \tag{4.2}$$

where, $C(n)$ is a number that depends on the mode of vibration of the rod. The condition on the time and space step is essentially stating that the simulation must run faster than the transverse wave one wants to capture.

The boundary conditions for the selected problem are of the mixed kind. At the fixed end the angular and linear velocities are zero. That is, $v_1 = v_2 = v_3 = 0$ and $\omega_1 = \omega_2 = \omega_3 = 0$ at i = 1 for all j. At the free end, the force and moments are known and thus by the constitutive equation (3.4), force and the Darboux vector are known. That is, if the force and the moment at the free end are denoted respectively as $\bar{\mathbf{N}}$ and $\bar{\mathbf{M}}$, then at $i = NS$ for all j, $\mathbf{N}(NS, j) = \bar{\mathbf{N}}$ and $\mathbf{u}(NS, j) = \mathbf{B}^{-1}\bar{\mathbf{M}}$. At the initial condition, j = 1, the linear and angular velocities are zero and the rod is along the x-axis. That is, $\mathbf{v}(i,1) = \boldsymbol{\omega}(i,1) = \mathbf{u}(i,1) = \mathbf{0}$. The rod initially placed on the x-axis implies that the tangent to the rod, $\mathbf{d_3}$, is along the x-axis. Thus, desiring a right-handed coordinate system, $\mathbf{d_1}$ is chosen along the y-axis and $\mathbf{d_2}$ along the z-axis initially.

The central difference in space and forward difference in time used in the scheme are given as

$$\left.\frac{\partial a}{\partial s}\right|_{(i,j)} = a'(i,j) = \frac{a(i+1,j) - a(i-1,j)}{2\Delta s}$$
$$\left.\frac{\partial a}{\partial t}\right|_{(i,j)} = \dot{a}(i,j) = \frac{a(i,j+1) - a(i,j)}{\Delta t} \tag{4.3}$$

From here on, the dash over a vector denotes the partial differential in space and a dot denotes the partial differential in time.

Starting from the initial conditions, first the components of the Darboux vector, $\mathbf{u}$, are calculated using the compatibility equation (3.10) at the time step, $t = (j+1)\Delta t$ and at all space steps, $i = 1, 2, \ldots NS$.

$$\dot{\mathbf{u}}(i,\mathrm{j}) = \boldsymbol{\omega}'(\mathrm{i},\mathrm{j}) + \mathbf{u}(\mathrm{i},\mathrm{j}) \times \boldsymbol{\omega}(i,j) \tag{4.4}$$

$$\mathbf{u}(i,\mathrm{j}+1) = \mathbf{u}(i,\mathrm{j}) + \Delta t^{*}(\boldsymbol{\omega}'(\mathrm{i},\mathrm{j}) + \mathbf{u}(\mathrm{i},\mathrm{j}) \times \boldsymbol{\omega}(i,j)) \tag{4.5}$$

The frame of directors, $\{\mathbf{d_1}, \mathbf{d_2}, \mathbf{d_3}\}$ at each point in space for the time step, $t = (j+1)\Delta t$ are calculated by integrating the equation $(3.1)_1$. The integration results in a matrix exponential [9] and this can also be written as the Rodrigues rotation matrix. [21].

$$\mathbf{R}_i^{j+1} = \mathbf{I} + \tilde{\mathbf{u}}_i^{j+1} \sin \Delta \mathrm{s} + (\tilde{\mathbf{u}}_i^{j+1})^2 (1 - \cos \Delta \mathrm{s}) \tag{4.6}$$

$$\begin{Bmatrix} \boldsymbol{d_3} \\ \boldsymbol{d_1} \\ \boldsymbol{d_2} \end{Bmatrix}_{i+1}^{j+1} = \mathbf{R}_i^{j+1} \begin{Bmatrix} \boldsymbol{d_3} \\ \boldsymbol{d_1} \\ \boldsymbol{d_2} \end{Bmatrix}_{i}^{j+1} \tag{4.7}$$

With $\tilde{\mathbf{u}}_i^{j+1}$ being the skew symmetric matrix of the vector $\mathbf{u}(i, j+1)$, given as

$$\tilde{\mathbf{u}} = \begin{bmatrix} 0 & -u_2 & u_1 \\ u_2 & 0 & -u_3 \\ -u_1 & u_3 & 0 \end{bmatrix} \tag{4.8}$$

Then, the components of the linear velocity vector, $\mathbf{v}$, at all space points, i = 1, 2, … *NS*, and at time, $t = (j+1)\Delta t$ are calculated using the constraint equation (3.14) as:

$$\mathbf{v}'(i, j+1) = \boldsymbol{\omega}(i, j+1) \times \mathbf{d}_3(i, j+1) - \mathbf{u}(i, j+1) \times \mathbf{v}(i, j+1). \tag{4.9}$$

$$\mathbf{v}(i+1, j+1) = \mathbf{v}(i-1, j+1) + 2 * \Delta s * (\boldsymbol{\omega}(i, j+1) \times \mathbf{d}_3(i, j+1) - \mathbf{u}(i, j+1) \times \mathbf{v}(i, j+1)). \tag{4.10}$$

The angular velocity is calculated next at all space points, i = 1, 2, … *NS*, and at time step, $t = (j+1)\Delta t$ using the equations below. These equations follow from the governing equation $(3.6)_2$.

$$\begin{aligned} \tilde{\mathbf{I}}.\dot{\boldsymbol{\omega}}(i, j) = \mathbf{d}_3(i, j) \times \mathbf{N}(i, j) + \mathbf{L}(i, j) - \boldsymbol{\omega}(i, j) \times \left(\tilde{\mathbf{I}}.\boldsymbol{\omega}(i, j)\right) ... \\ ... + \mathbf{Bu}'(i, j+1) + \mathbf{u}(i, j+1) \times \left(\mathbf{Bu}(i, j+1)\right). \end{aligned} \tag{4.11}$$

$$\begin{aligned} \tilde{\mathbf{I}}.\boldsymbol{\omega}(i, j+1) = \tilde{\mathbf{I}}.\boldsymbol{\omega}(i, \mathrm{j}) + \Delta t * (\mathbf{d}_3(i, j) \times \mathbf{N}(i, j) + \mathbf{L}(i, j) - \boldsymbol{\omega}(i, j) \times \left(\tilde{\mathbf{I}}.\boldsymbol{\omega}(i, j)\right) ... \\ ... + \mathbf{Bu}'(i, j+1) + \mathbf{u}(i, j+1) \times \left(\mathbf{Bu}(i, j+1)\right)). \end{aligned} \tag{4.12}$$

The next step is to calculate the components of the shear force and the axial force at all the space points, i = 1, 2, … *NS*, and at $t = (j+1)\Delta t$. This is done using the governing equation $(3.6)_1$.

$$\mathbf{N}'(i, j+1) = m\dot{\mathbf{v}}(i, j+1) + m(\boldsymbol{\omega}(i, j+1) \times \mathbf{v}(i, j+1)) - \mathbf{u}(i, j+1) \times \mathbf{N}(i, j+1) - \mathbf{T}(i, j+1). \tag{4.13}$$

$$\begin{aligned} \mathbf{N}(i+1, j+1) = \mathbf{N}(i-1, j+1) + 2\Delta s * (m\dot{\mathbf{v}}(i, j+1) + m(\boldsymbol{\omega}(i, j+1) \times \mathbf{v}(i, j+1)) ... \\ ... - \mathbf{u}(i, j+1) \times \mathbf{N}(i, j+1) - \mathbf{T}(i, j+1)). \end{aligned} \tag{4.14}$$

With the above equations, the 4 unknown vectors are calculated. At each time step, to obtain the position of the rod, equation (3.12) is integrated. That is, using the

condition that the cross-sections do not shear, the tangent at each point, in this case, $\mathbf{d}_3$, can be integrated to get the position of the centerline of the rod.

$$\mathbf{R}'(i, j+1) = \mathbf{d}_3(i, j+1). \tag{4.15}$$

$$\mathbf{R}(i+1, j+1) = \mathbf{R}(i-1, j+1) + 2\Delta s * (\mathbf{d}_3(i, j+1)). \tag{4.16}$$

To be able to visualize the effect of twisting moment on the rod, the positions of an imaginary line on the periphery of the rod are calculated. This is done using the position of the centerline and the twist component of the Darboux vector. Integrating the twist component, the angle of twist can be obtained. And then the position of the peripheral line is calculated by a simple rotation of the centerline through the angle of twist. The peripheral line chosen is initially along the x-axis at a radial distance from the centerline along the z-axis. That is, at the space point i = 1, the coordinate of the point on the peripheral line is (0, 0, d/2). As stated before, d is the diameter of the rod. Suppose the position of the imaginary peripheral line is denoted as $\mathbf{R}_{end}$. Then, the 3 components of $\mathbf{R}_{end}$ at each point in space are calculated as shown below.

$$\begin{aligned}
&\mathbf{R}_{end}(1, i, j+1) = \mathbf{R}(1, i+1, j+1). \\
&\mathbf{R}_{end}(2, i, j+1) = \mathbf{R}(2, i+1, j+1) - \frac{d}{2}\sin(\Delta s * i * \mathbf{u}_3(i, j+1)). \\
&\mathbf{R}_{end}(2, i, j+1) = \mathbf{R}(2, i+1, j+1) + \frac{d}{2}\cos(\Delta s * i * \mathbf{u}_3(i, j+1)).
\end{aligned} \tag{4.17}$$

5. RESULTS[*]

The results of the simulation using the method described in the previous section are presented in this section for different plausible scenarios. Ramped and impulse inputs at the free end are considered and the results validated through analytical results. It is to be noted that the scheme presented in the previous section can be used only where the boundary conditions are of the mixed kind.

5.1 Preliminaries

The simulations are performed for a rod with properties listed in the table below. The table includes the properties entered as inputs to the program and the properties calculated based on formulae stated in the previous section.

Table 1: Table with properties and their values.

Property	**Value**
Input Properties	
Length, *L*	1.00 m
Diameter, *d*	0.001 m
Density, ρ	850.00 kg/m^3

[*] Parts of this chapter have been reprinted with the permission from "Modeling the dynamics of filaments for medical applications", by Nuti S., Ruimi A., Reddy J., 2014, *International Journal of Non-Linear Mechanics*, 66 (2014), 139-148, Copyright [2014] by Elsevier.

Table 1 Continued.

Property	Value
Modulus of Elasticity, E	87.50 MPa
Modulus of Rigidity, G	31.25 MPa
Poisson's ratio, υ	0.40
Total time, T	10.00 s
Number of points in space, NS	51
Transverse wave speed, c_T	0.882 m/s
Calculated Properties	
Space step, Δs	0.02 m
Time step, Δt	0.0166 s
Bending stiffness, B_1 and B_2	0.4295×10^{-5} N-m^2
Torsional stiffness, C	0.3068×10^{-5} N-m^2

5.2 Simulation Results

Each iteration took approximately 0.03 s CPU time on a laptop with Intel® Core™ i-3-3110M, 2.4Hz and 4GB RAM. This is about 5 times faster than the generalized-$\propto$ method with relaxation method as performed by Sobottka, Lay and Weber [9].

The final configurations of the rod (i.e., at the last time step) for various inputs of force and moment at the free end are shown in figure 3 below. Note that the rod is fixed in space at the (0,0,0) point and is initially placed along the x-axis.

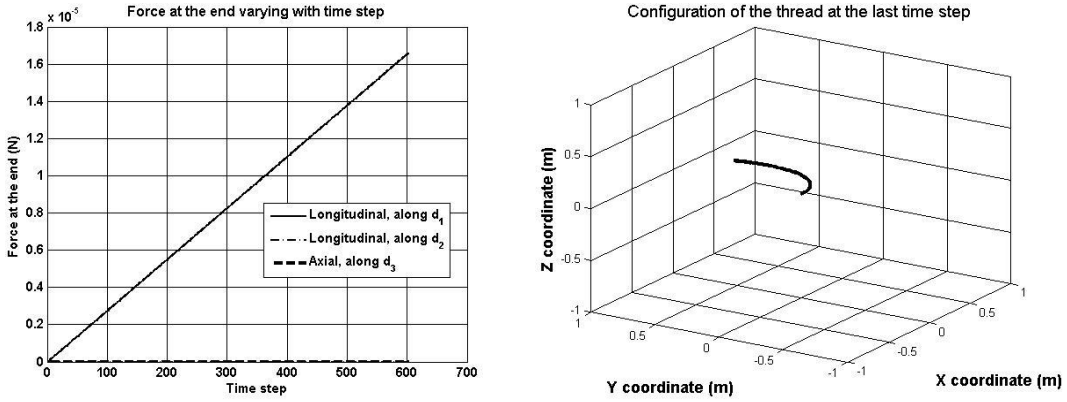

(a)

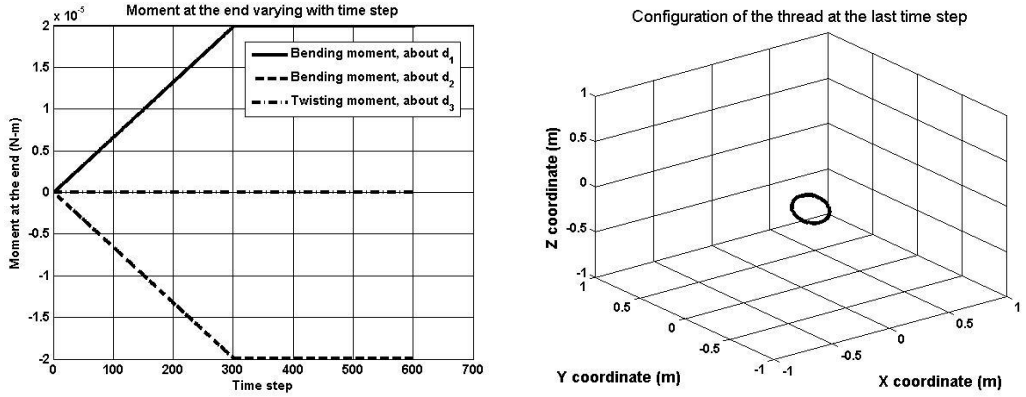

(b)

Figure 3: Snapshots of the filament's final configuration (right) (at the last time step) for different inputs (left): (a) Only N_1 [22], (b) M_1 and M_2 [23].

The results for the transverse load are validated using analytical results. As can be seen in table 2, the results are very similar.

Next, the effects of axial force and of twist are observed. These inputs are slowly increased till buckling is observed. The results are as shown in figure 4.

Table 2: Analytical vs simulated results.

Force at the free end, P (N)	Simulated end deflection, y_{sim} (m)	Expected end deflection, $y_{exp} = PL^3/3EI$ (m)	%error = $\frac{y_{exp}-y_{sim}}{y_{exp}} \times 100$
4.50E-07	0.0352	0.0349	-0.792%
8.00E-07	0.0627	0.0621	-0.763%
1.00E-06	0.0782	0.0776	-0.989%

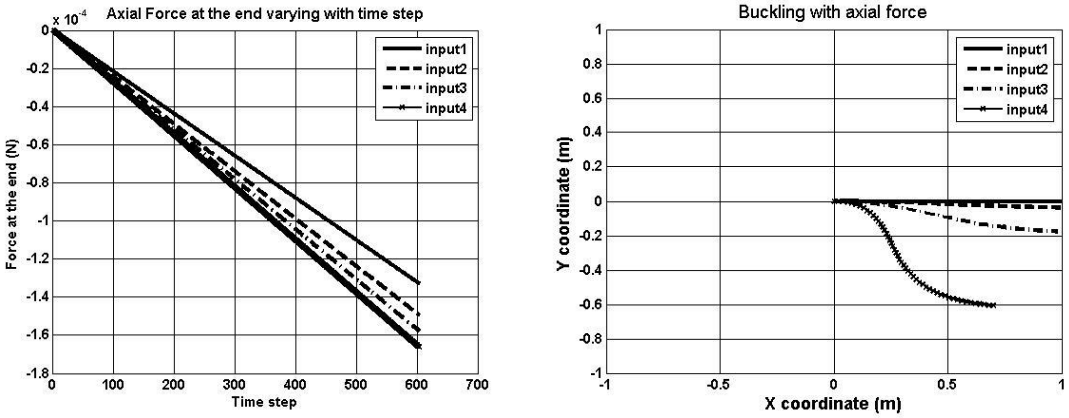

(a)

Figure 4: Buckling of the rod under: (a) Axial force [24], (b) Twisting moment [25].

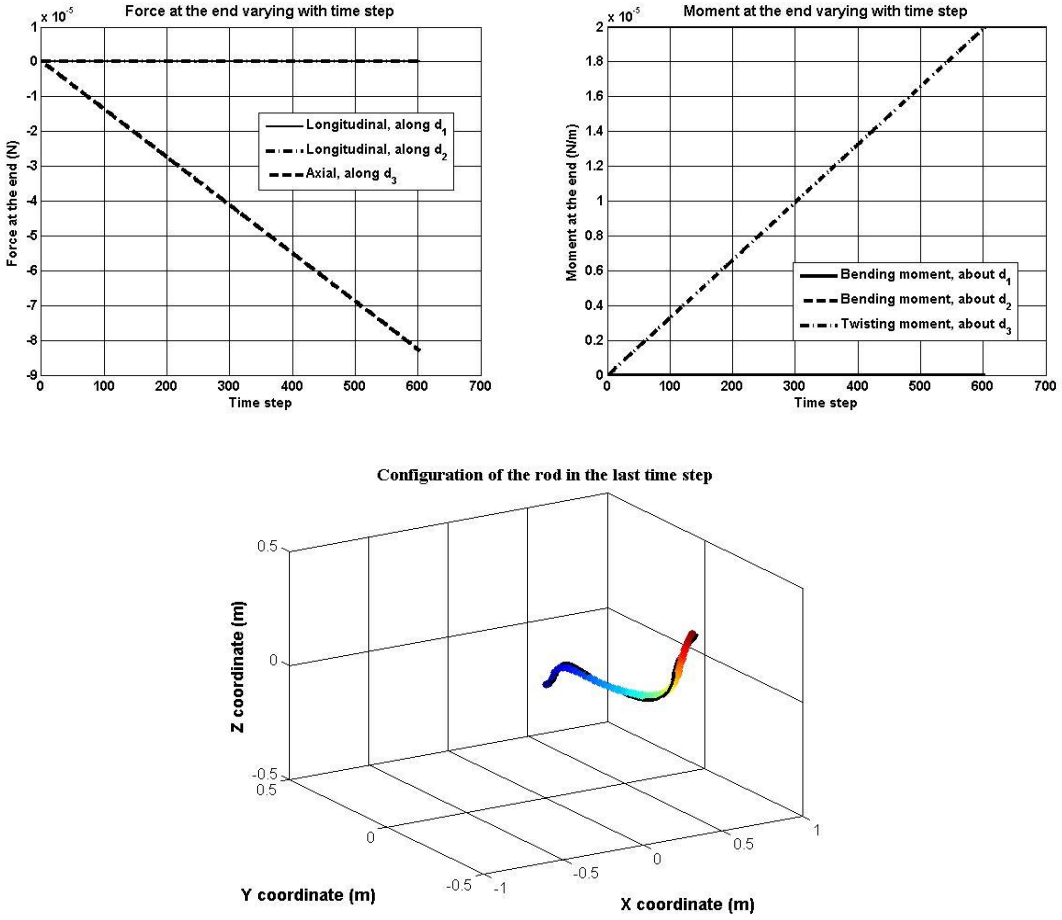

(b)

Figure 4 Continued.

The effects of different rod parameters on buckling due to axial force and twisting moment are recorded. The effect of the parameters on buckling due to twist is stated below.

For different moduli of elasticity, the final configurations of the rod are compared. It is seen that the lower the elastic modulus, the greater the buckling. This can

be explained as the rod taking the configuration of least energy. With a smaller elasticity modulus, the energy for bending is smaller. Hence, the rod would prefer to bend than to remain twisted. The figure below shows the configuration of the rod at the last time step with different elasticity modulus for the same axial force.

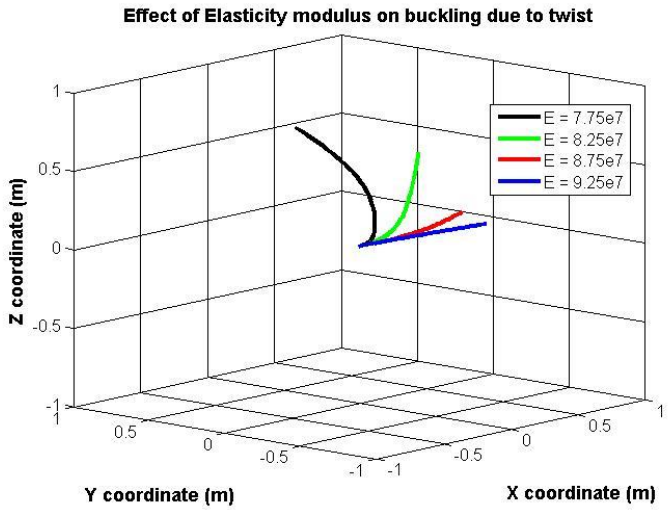

Figure 5: Effect of elasticity modulus on buckling due to twist.

For different lengths of the rod, it is interesting to note that a shorter rod buckles faster than a longer rod as can be seen in the figure 6. This is probably due to the twist distribution along the length of the rod. A shorter rod undergoes more twist than a longer rod and hence buckles faster.

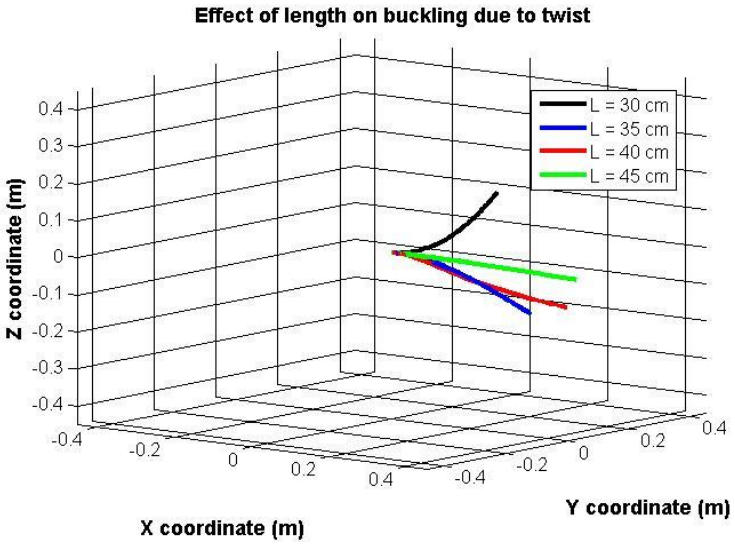

Figure 6: Effect of length on buckling due to twist.

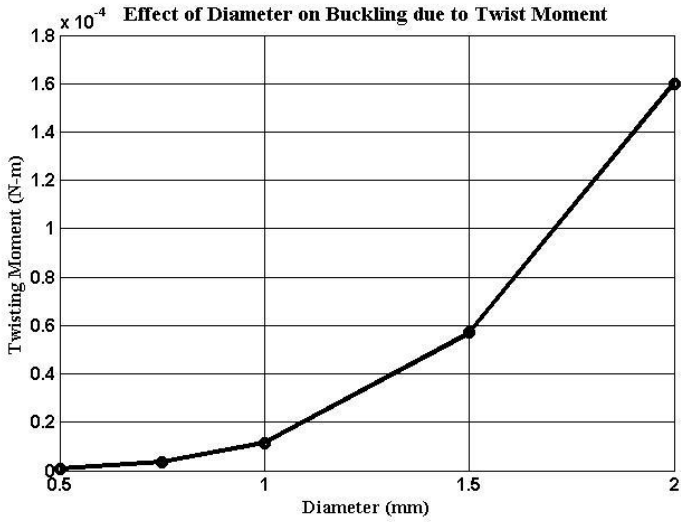

Figure 7: Effect of rod diameter on twisting moment causing buckling.

When the diameter is increased, it is seen that a higher twisting moment is required to buckle the rod. Figure 7 above shows the effect of the diameter on the buckling due to twisting moment.

Looking at the effects of diameter and length on the buckling of the rod due to axial load, it can be seen from figure 8 that a longer rod buckles at a lower force than a shorter rod. This is because the longer rod is less stiff than the shorter rod. Similarly, a thinner rod buckles at a lower force. Both these parameters affect the stiffness of the rod and hence the buckling. The effect of the diameter on the buckling due to axial force is shown in figure 9.

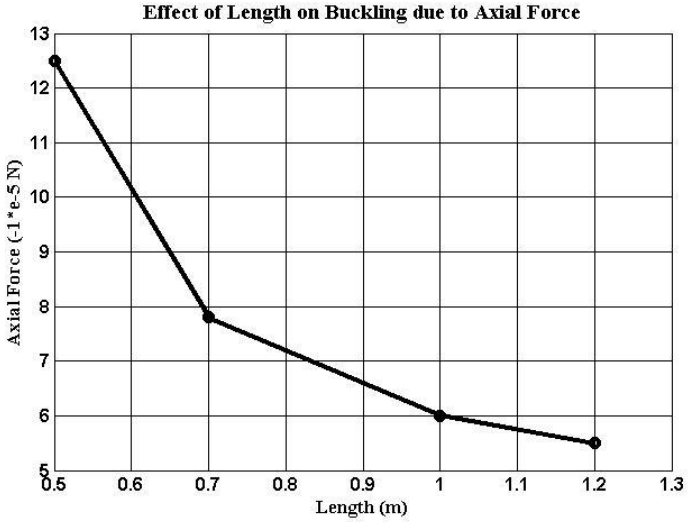

Figure 8: Effect of rod length on axial force required to buckle the rod.

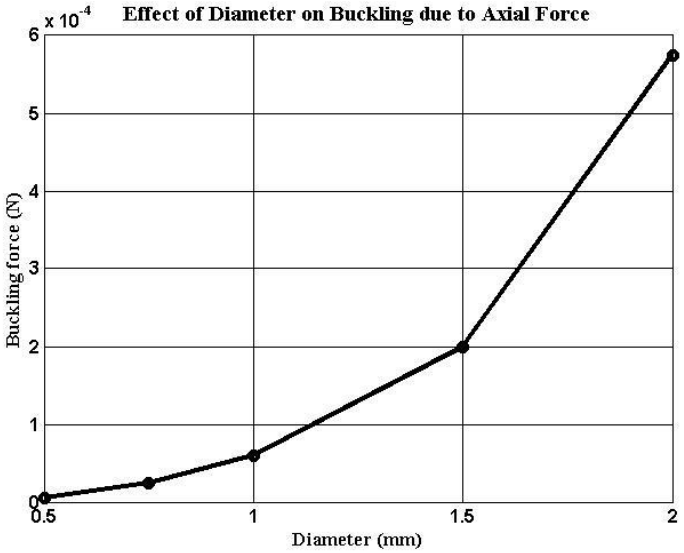

Figure 9: Effect of diameter on the axial force required to buckle the rod.

The results for an impulse type input are shown in figure 10. A transverse force of magnitude N_1 = 0.25 N is applied for Δt = 0.005 s followed by a load of the same magnitude but opposite in direction for the same duration. The rod's configurations at different instances of time are shown in the figure and it can be seen that the rod vibrates with different modes excited. The results are validated by comparing the plot of the rod's displacements at different points in space and time to those obtained analytically [26, 27]. This is shown in figure 11. An FFT analysis of the motion of the rod at the free end and at the mid-point, obtained from the numerical and analytical methods, is shown in figure 12 and figure 13, respectively. The results show a strong agreement between predicted and simulated results. The numerical results, however, show small peaks at frequencies just beyond 2 Hz whereas the analytical results show a smooth curve.

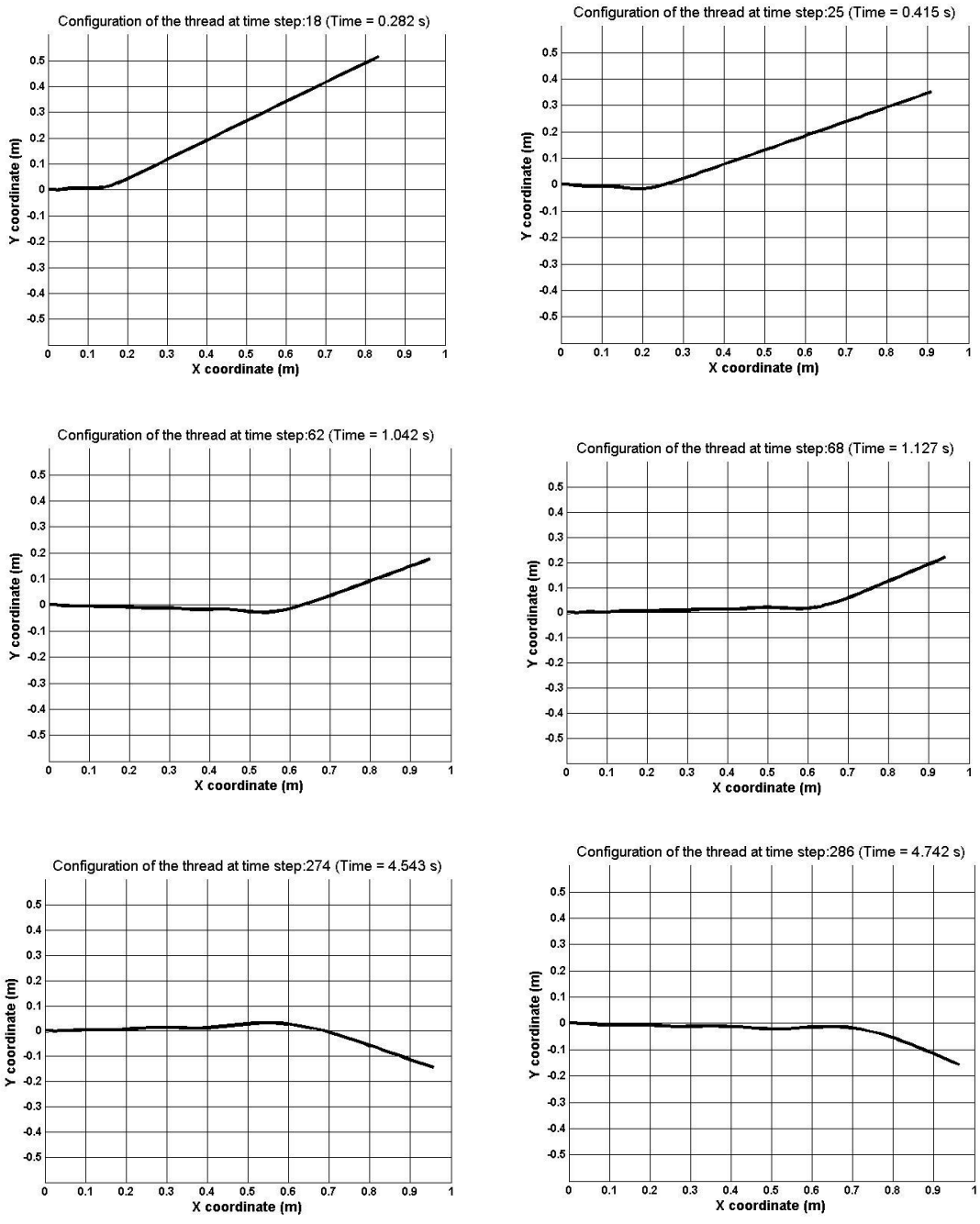

Figure 10: Transient response of the rod due to an impulse force [28].

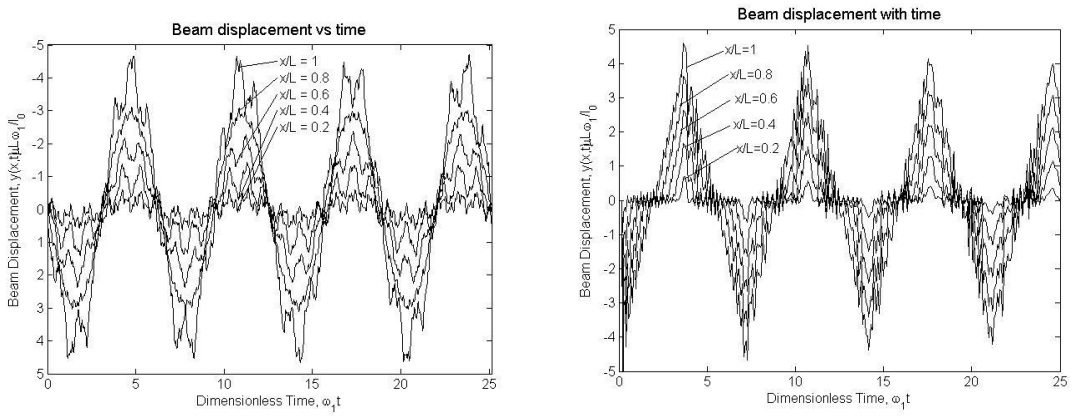

Figure 11: Predicted values of displacement as a function of time (left) and simulated values (right).

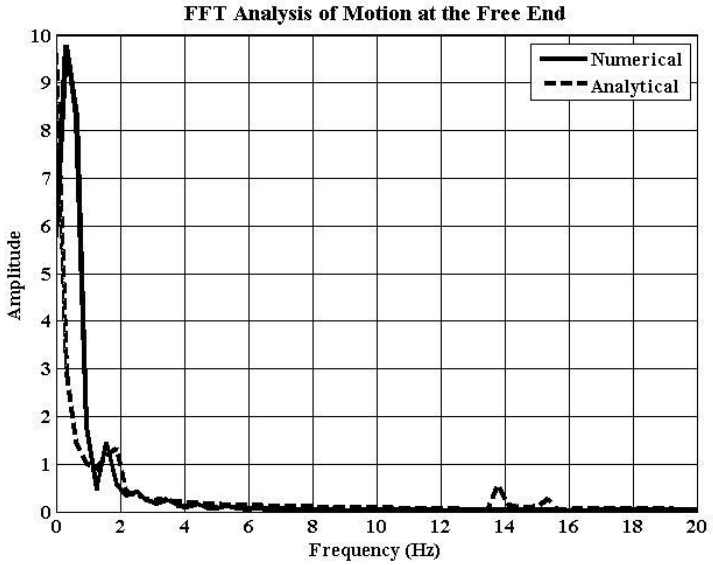

Figure 12: FFT analysis of motion at free end of the rod.

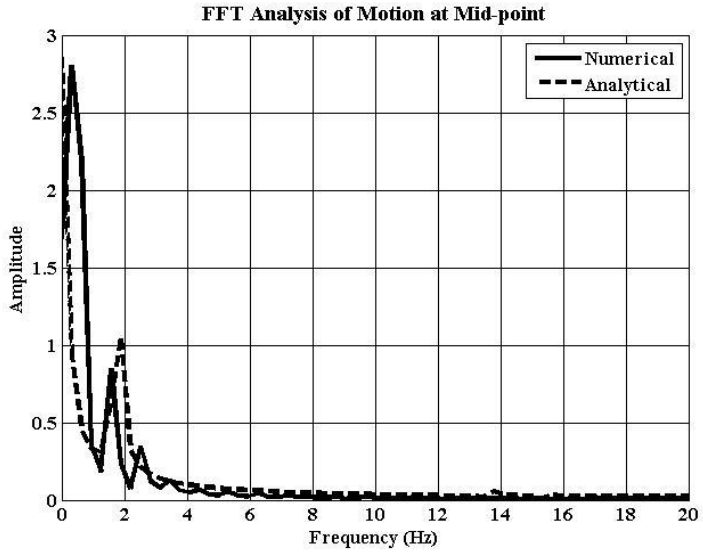

Figure 13: FFT analysis of motion at mid-point of the rod.

It is important to note that twist waves run faster than transverse waves and hence require a much smaller time step to be captured. The time step used to capture twisting is about ten times smaller than that used for bending. This is a disadvantage of this conditionally stable scheme.

It is shown in this section that the numerical results are in good agreement with the analytical results. Even though its conditional stability affects its speed when twist waves are considered, the simplicity of the scheme makes it faster than most other schemes. Thus the scheme would hold great advantages in real-time simulations.

6. CONCLUSION

In brief, the dynamics of slender rods is represented using the theory of Cosserat rod and solved using finite difference method. The simulation scheme has not been used before and is central difference in space and forward difference in time. The positions of the rod at any given time are calculated using incremental angles.

The simulations have been performed for a cantilever rod that is fixed at one end and whose other end is subjected to forces and moments. The results have been compared to analytical results and found to be in good agreement. Buckling effects due to axial force and twisting moment and effects of different parameters of the rod on the same have also been observed.

As an extension, in the future, the application of this scheme on boundary conditions other than the cantilever kind may be explored. Also, modifying the scheme to make it unconditionally stable is another avenue to be looked into. Using the simulation scheme, an interactive program may be developed where the inputs to the free end of the rod are measured in real-time through sensors and fed as inputs from the hand of the user to the program. This will be the first step in creating a software that can help medical students train in the act of suturing.

REFERENCES

[1] Ncbi.nlm.nih.gov, (2014), "Home - PubMed – NCBI", [online] Available at: http://www.ncbi.nlm.nih.gov/pubmed/, Accessed 20 Nov 2014.

[2] Berkley, J., Weghorst, S., Gladstone, H., Raugi, G., Berg, D., Ganter, M., "Banded matrix approach to finite element modeling for soft tissue simulations", *Virtual Reality* 4(3) (1999), 203-212.

[3] Reddy, J. N., *Energy Principles and Variational Methods in Applied Mechanics*, 2nd ed., John Wiley & Sons, New York (2002).

[4] Carrera, E., Giunta, G. and Petrolo, M., *Beam Structures: Classical and Advanced Theories*, John Wiley & Sons, New Jersey (2011).

[5] Dill, E. H, "Kirchhoff Theory of Rods", *Archive for History of Exact Sciences* 44(1) (1992), 1-23.

[6] Altenbach, H., and Eremeyev. V. A. (eds.), *Generalized Continua from the Theory to Engineering Applications*. Springer-Verlag Wien, CISM (Udine), (2013) 179-248.

[7] Pai, D. K., "STRANDS: Interactive simulation of thin solids using Cosserat models", *Computer Graphics Forum*, 21(3) (2002), 347-352.

[8] Goyal, S., Perkins, N. C., and Lee, C. L. "Nonlinear dynamics and loop formation in Kirchhoff rods with implications to the mechanics of DNA and cables", *Journal of Computational Physics*, 209 (2005) 371–389.

[9] Sobottka, G., Lay, T., and Weber, A., "Stable integration of the dynamic Cosserat equations with application to hair modeling", *Journal of WSCG 16* (1-3) (2008), 73-80.

[10] Gobat, J. and Grosenbaugh, M., "Application of the generalized-alpha method to the time integration of the cable dynamics equations", *Computer Methods in Applied Mechanics and Engineering*, 190 (37-38) (2001), 4817-4829.

[11] Reddy, J. N., *An Introduction to Nonlinear Finite Element Analysis*, Oxford University Press, Oxford, UK (2015).

[12] Holger, L., Linn, J., and Arnold, M., "Multi-body Dynamics Simulation of Geometrically Exact Cosserat Rods", *Multibody System Dynamics*, 25(3) (2011), 285-312.

[13] Spillmann, J. and Teschner, M., "CORDE: Cosserat Rod Elements for the Dynamic Simulation of One-Dimensional Elastic Objects", in *Proceedings of the ACM SIGGRAPH/Eurographics Symposium on Computer Animation*, San Diego, USA, 1 (2007) 209-217.

[14] Cao, D.Q., Liu, D., and Wang, C. H.-T., "Three-dimensional Nonlinear Dynamics of Slender Structures: Cosserat Rod Element Approach", *International Journal of Solids and Structures*, 43 (3-4) (2006) 760-783.

[15] Berkley, J., Turkiyyah, G., Berg, D., Ganter, M., and Weghorst, S., "Real-time finite element modeling for surgery simulation: an application to virtual

suturing", *IEEE Transactions on Visualization and Computer Graphics*, 10 (2004) 314-325.

[16] Brown, J., Latombe, J. C., and Montgomery, K., "Real-time knots tying simulation", *The Visual Computer* 20(2-3) (2004) 165-179.

[17] Wang, F., Burdet, E., Dhanik, A., Poston, T., Teo, C.L., "Dynamic thread for real time knot-tying", in *Proceedings of the First Joint Eurohaptics Conference and Symposium on Haptic Interfaces for Virtual Environment and Teleoperator Systems* (2005) 507-508.

[18] Hadap, S., and Magnenat-Thalmann, N., "Modeling Dynamic Hair as a Continuum", *Computer Graphics Forum*, 20(3) (2001), 329-338.

[19] Lenoir, J., Meseure, P., Grisoni, L., and Chaillou, C., "A suture model for surgical simulation", in *Proceedings of International Symposium on Medical Simulations*, S. Cotin and D. Metaxas (eds.), Springer-Verlag, Berlin (2004) 105-113.

[20] Survinat.com, (2014), "Surgical Sutures", The survival encyclopedia, [online] Available at: http://survinat.com/2012/08/surgical-sutures/, Accessed 21 Nov. 2014.

[21] Electroncastle.com, (2014), "Matrix exponential to the Rodrigues' rotation formula", Electron Castle, [online] Available at: http://electroncastle.com/wp/?p=493, Accessed 21 Nov. 2014.

[22] Nuti, S. (2014), "only longitudinal force along d1, N1 output", YouTube, [online] Available at: http://youtu.be/MMyBNzHhsog, Accessed 21 Nov. 2014.

[23] Nuti, S. (2014), "Bending moments about d1 and d2, M1 and M2, output", YouTube, [online] Available at: http://youtu.be/YBjOb8-s_h4, Accessed 21 Nov. 2014.

[24] Nuti, S. (2014), "buckling with axial force", YouTube, [online] Available at: http://youtu.be/WqR0oGMRpHY, Accessed 21 Nov. 2014.

[25] Nuti, S. (2014), "buckling with twist", YouTube, [online] Available at: http://youtu.be/1HPhAv1N0ms, Accessed 21 Nov. 2014.

[26] Ginsberg, J. H., *Mechanical and Structural Vibrations: Theory and Applications*, New York: J. Wiley & Sons (2001).

[27] Uwyo.edu, (2014), "Index to Animation Scripts | College of Engineering and Applied Science | University of Wyoming", [online] Available at: http://www.uwyo.edu/ceas/current-students/classes/matlabanimate/index.html#Beam%20Vibration, Accessed 21 Nov. 2014.

[28] Nuti, S. (2014), "impulse force output 2", YouTube [online], Available at: http://youtu.be/YU-oQEiAJLY, Accessed 21 Nov. 2014.